A Deep Learning Approach for Semantic, Multi-Organ Segmentation of PET Images

Joshua Schaefferkoetter, *Member, IEEE*, Paul Schleyer, *Member, IEEE*, Maurizio Conti, *Member, IEEE*

Introduction

Semantic segmentation refers to the classification of each pixel in an image according to contextual information. In the medical setting, image segmentation tasks include organ identification, tissue classification and disease detection. Reliable methods to automatically perform such tasks would offer unprecedented advantages for assisting radiologic interpretation and efficiency in routine clinical workflows. Currently, algorithms based on convolutional neural networks (CNNs) are state-of-the-art for segmentation tasks and have seen huge success for a wide range of medical applications – largely focused on high resolution, anatomical modalities like CT and MRI.

Nuclear medicine modalities like PET and SPECT have received much less attention but have seen some efforts focused on specific tasks like the identification of acute pathology and lesion detection [1]. Far fewer studies have investigated the capacity of a CNN to perform a more general segmentation task, delineating multiple organs directly on PET images [2]. Such a segmentation approach could open new avenues for image processing and tissue-specific analyses, and the work presented here investigated this in the context of whole- and total-body imaging with various PET tracers.

Methods

Network architecture

A standard 3D U-Net was chosen for this work [3]. It used 64 feature channels at the highest-resolution blocks and with increasing numbers at each down-sampled level. Instance normalization was used throughout, with a soft Dice loss. The training objective was minimized by the Adam optimizer [4] with a learning rate of 10^{-4}. The final network had ~19M trainable parameters.

Data preparation and training

A set of labeled training data was generated in the following way. A dataset including ~1400 human subjects was first obtained which comprised CT image volumes and matched segmentation labels corresponding to 104 anatomical regions [5]. These class labels were used to derive a smaller set of 60 target regions considered to be relevant for PET image data, which were then used as the final training labels for the CT volumes. The list of all anatomical regions is given in Table 1.

TABLE I

Anatomical regions included in the segmentation

1	aorta	16	patella	31	scapula	46	vert L3
2	bladder	17	radius	32	skull	47	vert L4
3	brain	18	rib 1	33	spleen	48	vert L5
4	clavicle	19	rib 2	34	sternum	49	vert T1
5	femur	20	rib 3	35	tibia	50	vert T2
6	fibula	21	rib 4	36	ulna	51	vert T3
7	foot	22	rib 5	37	vert C1	52	vert T4
8	hand	23	rib 6	38	vert C2	53	vert T5
9	heart	24	rib 7	39	vert C3	54	vert T6
10	hip	25	rib 8	40	vert C4	55	vert T7
11	humerus	26	rib 9	41	vert C5	56	vert T8
12	intestine	27	rib 10	42	vert C6	57	vert T9
13	kidney	28	rib 11	43	vert C7	58	vert T10
14	liver	29	rib 12	44	vert L1	59	vert T11
15	lung	30	sacrum	45	vert L2	60	vert T12

A CNN was trained to perform the CT segmentation for ~200k iterations. The trained algorithm was subsequently used to label a new set of whole-body CT volumes from subjects scanned on a PET/CT, and so each had an accompanying PET image. The labels were inspected and refined as needed. A new CNN was trained using the new labeled images to perform the segmentation task directly on the PET images. Three different tracers were included together in the training pool: 18F-FDG, 68Ga-PSMA and 68Ga-DOTATATE.

Results

Two subjects were reserved solely for testing and evaluation: 1 FDG and 1 PSMA. The performance of the PET segmentation algorithm was compared to that of the CT segmentation in both subjects. For the results reported here, the organs segmented on CT data were used as ground truth and served as the standard against which the PET segmentation was evaluated. Visually, the segmentations defined on the PET images appeared to be of good quality. Figure 1 provides an overview of the performance of the 2 segmentation algorithms for both test subjects.

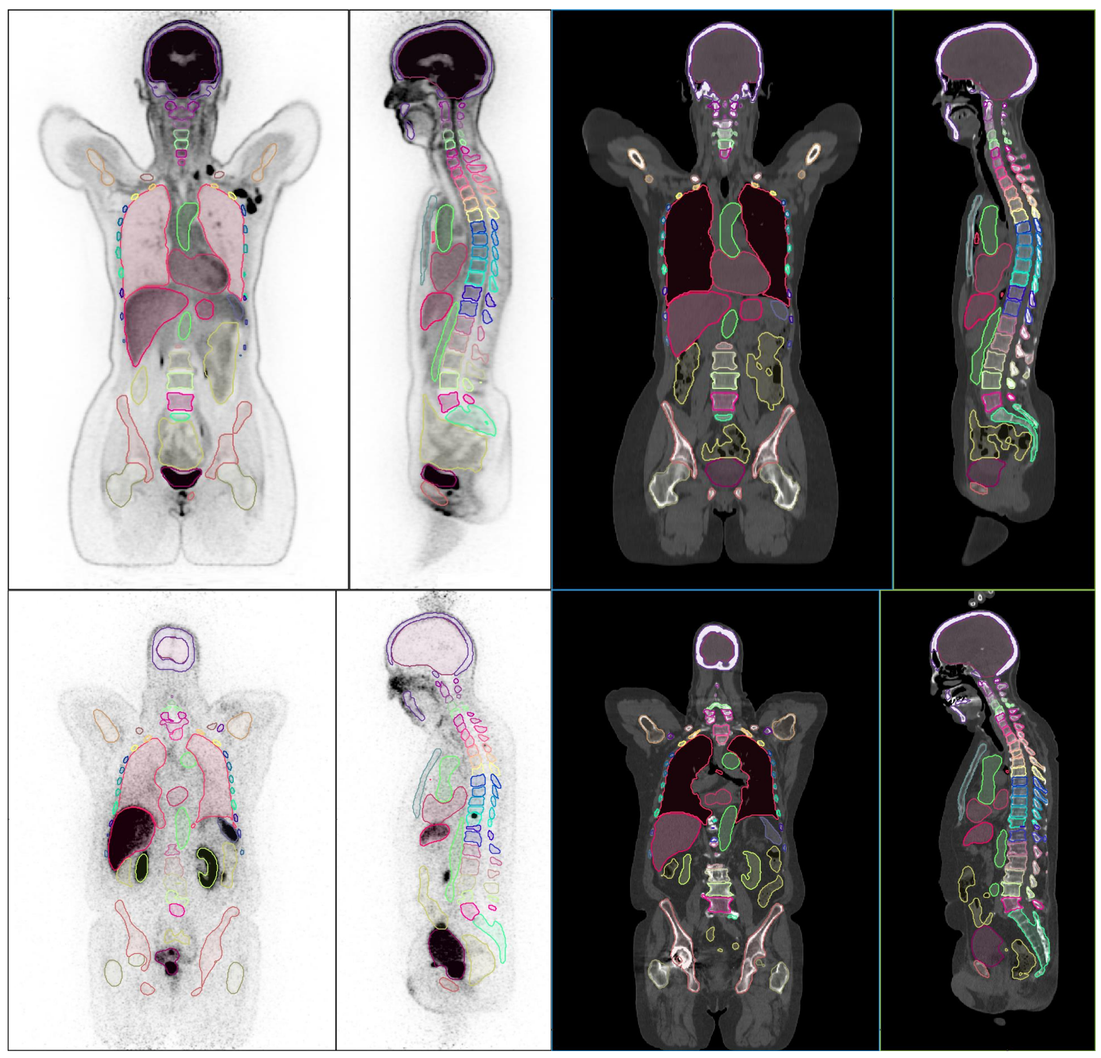

Fig. 1. Visual overview of the segmentations defined by the PET algorithm (left) and by those defined by the CT algorithm (right). These 2 subjects were scanned with different PET tracers, FDG on top and PSMA on bottom.

Accuracy of the PET segmentation is quantified here by the total Dice similarity over all CT segmentations, as well as averaged over the individual organ classes, for each patient individually. For the FDG case, the total and class-averaged Dice scores were 0.83 and 0.71, respectively, and for the PSMA case, the Dice scores were 0.74 and 0.47, respectively.

Discussion

A single network demonstrated the capacity to perform segmentations on PET image volumes for many organ classes simultaneously. Furthermore, a single network was able to handle multiple radiotracers. The defined segmentations appeared to be of high quality, with good morphological characteristics for all visualized organ regions. This was notably impressive for the more specific tracers, like PSMA, where, even in the large regions with sparse uptake, e.g., around the thoracic and abdominal spinal column, the algorithm was able to generate reasonable segmentations using only the surrounding contextual information. The quantitative evaluation also revealed good concordance between the regions delineated on the PET and those delineated on the CT. This was observed for both PET tracers, although the FDG image yielded more accurate segmentations compared to the PSMA image, relative to those defined on CT.

There are notable limitations in using the CT segmentations as ground truth, since the PET and CT were acquired at different time points and there is no guarantee that the 2 image volumes are spatially matched across the entire body. Positional misalignment between the images would result in a lower Dice score, even with perfect performance of the segmentation algorithms. This consideration is motivating the search for other appropriate evaluation metrics to be used in future work.

Disclosure

All authors are full time employees of Siemens Medical Solutions USA, Inc., 810 Innovation Drive, Knoxville, TN 37932, USA

References

[1] Guo, H., et al. (2022). Investigation of small lung lesion detection for lung cancer screening in low dose FDG PET imaging by DNNs. *Frontiers in Public Health*.
[2] Xue, Song, et al. "CT-free Total-body PET segmentation." (2023): P833-P833.
[3] Ronneberger, O., et al. (2015). U-net: Convolutional networks for biomedical image segmentation. In *MICCAI* 2015: Proceedings, Part III 18 (pp. 234-241). Springer Publishing.
[4] Kingma, D. P., & Ba, J. (2014). Adam: A method for stochastic optimization. *arXiv*:1412.6980.
[5] Wasserthal, J., et al. (2023). Totalsegmentator: Robust segmentation of 104 anatomic structures in CT images. *Radiology: AI*, 5(5).